Journal of Wind Engineering & Industrial Aerodynamics 236 (2023) 105376

Contents lists available at ScienceDirect

Journal of Wind Engineering & Industrial Aerodynamics

journal homepage: www.elsevier.com/locate/jweia

Thunderstorm gust response factor: General tendencies and sensitivity analysis

Luca Roncallo *, Federica Tubino

Department of Civil, Chemical and Environmental Engineering (DICCA), Polytechnic School, University of Genoa, Via Montallegro 1, 16145, Genoa, Italy

ARTICLE INFO

Keywords:
Evolutionary spectral model
Gust response factor
Nonstationary dynamic response
Sensitivity analysis
Thunderstorm outflows

ABSTRACT

This paper aims to provide a sensitivity analysis of the thunderstorm gust response factor. The study is based on the extension of the gust response factor technique to the assessment of the maximum dynamic response of structures to thunderstorm outflows, starting from an evolutionary spectral model of the thunderstorm wind speed. The thunderstorm evolutionary spectral model depends on the modulating function of the slowly-varying mean speed, which is a function of two parameters, i.e. the background mean wind speed and the duration of the intense phase of the outflow. Starting from 129 full-scale thunderstorm records, the parameters of three different analytical models of the modulating function are extracted and a statistical analysis is carried out defining their range of variation. The dependence of the gust response factor on the analytical expression of the modulating function is studied as well as its sensitivity to the parameters of the function. Results show that the dependence of the gust response factor on the analytical expression of the modulating function is negligible, while it is very sensitive to the variation of the background wind and duration of the intense phase, especially for flexible and lowly-damped systems.

1. Introduction

The occurrence of extra-tropical cyclones and thunderstorm downbursts characterises the wind climate of several locations worldwide, threatening the durability and safety of the built environment.

While codes and standards provide suitable tools for engineers to deal with the wind-resistant structural design related to extra-tropical cyclones (Solari, 1983, 1993; Zhou and Kareem, 2001), which are mainly based on the gust factor technique from Davenport (1967), thunderstorm winds still lack of a suitable approach for the estimate of the wind loading and dynamic response shared by the scientific community. The growing desire to follow the consolidated approach for synoptic winds, eventually adapting the gust factor technique to thunderstorm outflows, urged researchers to adopt advanced techniques and develop new methods to characterize the wind loading and the maximum dynamic response induced by thunderstorms (Kwon and Kareem, 2009, 2013, 2019; Solari, 2016; Solari et al., 2015b).

In this framework, an Evolutionary Power Spectral Density (EPSD) model of thunderstorm outflows consistent with full-scale wind speed records was developed by Roncallo and Solari (2020). Two models for the modulating function of the slowly-varying mean wind speed were proposed, depending on two parameters with physical meaning: the background wind and the duration of the intense phase of the thunderstorm. Successively, Roncallo et al. (2022) adopted the EPSD model to estimate the maximum dynamic response of linear SDOF systems through the Equivalent Parameters Technique (EPT) (Michaelov et al., 2001), coherently with the approach proposed by Kwon and Kareem (2019) and accounting for the transient dynamic effects due to the nonstationary loading. The gust response factor for synoptic winds was thus generalized to the case of thunderstorm outflows and the results were validated against the mean reduced Thunderstorm Response Spectrum (TRS) (Solari et al., 2015c), confirming that neglecting the transient dynamic effects can be overconservative.

Although the approach proposed in Roncallo et al. (2022) for the estimate of the maximum dynamic response shows a good agreement with the full scale records, it was validated assuming a couple of values of the parameters that allow to best trace the mean trend of the slowly-varying mean of the records available. The choice was justified by the aim of estimating the mean value of the maximum response, comparing the generalized gust response factor with the one derived from data in terms of mean reduced TRS. However, thunderstorms may be significantly different from one to another and hence the variation of

* Corresponding author.
E-mail address: luca.roncallo@edu.unige.it (L. Roncallo).

https://doi.org/10.1016/j.jweia.2023.105376
Received 26 August 2022; Received in revised form 2 March 2023; Accepted 4 March 2023
Available online 23 March 2023
0167-6105/© 2023 The Authors. Published by Elsevier Ltd. This is an open access article under the CC BY-NC-ND license (http://creativecommons.org/licenses/by-nc-nd/4.0/).

the parameters needs to be assessed, along with the investigation of the sensitivity of the gust response factor to such variation. This paper aims to address these problems by: investigating the sensitivity of the gust response factor to the analytical model chosen for the modulating function; defining the range of variation of the parameters of the modulating function through a statistical analysis starting from full-scale data; studying the tendency of the equivalent parameters varying the parameters and finally carrying out a sensitivity analysis of the gust response factor.

2. Analytical formulation and statistical analysis of the parameters

2.1. Analytical formulation

Let us consider the non-directional wind speed $v(t)$ provided by a thunderstorm outflow in a point in space, modelled as a uniformly modulated nonstationary random process (Roncallo and Solari, 2020):

$$v(t) = \bar{v}_{max}\gamma(t)[1 + I_v\tilde{v}'(t)] \tag{1}$$

where $t \in \left[-\frac{T_{max}}{2}, \frac{T_{max}}{2}\right]$ is the time, being $T_{max} = 600$ s the thunderstorm duration, $\bar{v}_{max}$ and $\gamma(t)$ are, respectively, the maximum value and the deterministic modulating function of the slowly-varying mean wind speed (Solari et al., 2015a), I_v the mean value of the turbulence intensity over T_{max} and $\tilde{v}'(t)$ the so-called reduced turbulent fluctuation, dealt with as a zero-mean stationary Gaussian random process with unitary standard deviation. This latter is statistically characterized by its Power Spectral Density (PSD) $S_{\tilde{v}'}(n)$ modelled according to Solari and Piccardo (2001):

$$S_{\tilde{v}'}(n) = \frac{1}{n}\frac{6.868nL_v/\bar{v}_{max}}{\left[1 + 10.302nL_v/\bar{v}_{max}\right]^{5/3}} \tag{2}$$

where n is the frequency and L_v the integral length scale (Roncallo and Solari, 2020; Zhang et al., 2018).

Let us now consider a linear elastic SDOF system characterized by mass m, fundamental circular frequency $\omega_0 = 2\pi n_0$ (being n_0 the natural frequency and $T_0 = 1/n_0$ the natural period) and damping ratio ξ. The structure can be schematized as a point-like surface with area A perpendicular to the wind velocity direction and drag coefficient c_D. Invoking the hypothesis of small turbulence and having defined $x(t)$ the alongwind displacement, the maximum response can be expressed as (Roncallo et al., 2022):

$$x_{max} = G_x\bar{x}_{max} \tag{3}$$

where $\bar{x}_{max}$ and G_x are, respectively, the maximum value of the mean part of the response and the gust response factor in its generalized form for thunderstorm winds:

$$\bar{x}_{max} = \frac{\rho\bar{v}_{max}^2 Ac_D}{2m(2\pi n_0)^2} \tag{4}$$

$$G_x = 1 + 2I_v g_x\left(\nu_{\tilde{x}'}\tilde{T}_{eq}\right)\tilde{J}\,\mathscr{C} \tag{5}$$

with g_x the Davenport peak factor (Davenport, 1964), $\nu_{\tilde{x}'}$ the expected frequency, $\tilde{T}_{eq}$ the non-dimensional equivalent period, $\tilde{J}$ the non-dimensional standard deviation of the dynamic response to the stationary part of the turbulence and $\mathscr{C}$ the normalized non-dimensional equivalent standard deviation (Roncallo et al., 2022). They are defined in non-dimensional form as follows:

$$\nu_{\tilde{x}'} = \sqrt{\frac{c_{11,\tilde{x}'}(\tilde{t}_0)}{c_{00,\tilde{x}'}(\tilde{t}_0)}} \tag{6}$$

$$\tilde{T}_{eq} = \int_{-\frac{\tilde{T}_{max}}{2}}^{+\frac{\tilde{T}_{max}}{2}} \exp\left[4 - \frac{4(2I_v)^2\tilde{J}^2\mathscr{C}^2}{c_{00,\tilde{x}'}(\tilde{t})}\right]d\tilde{t} \tag{7}$$

$$\tilde{J}^2 = \int_0^{+\infty} |\tilde{H}(\tilde{n})|^2\tilde{S}_{\tilde{v}'}(\tilde{n})d\tilde{n} \tag{8}$$

$$\mathscr{C}^2 = \frac{1}{(2I_v)^2\tilde{J}^2}\frac{\int_{-\frac{\tilde{T}_{max}}{2}}^{+\frac{\tilde{T}_{max}}{2}} c^5_{00,\tilde{x}'}(\tilde{t})d\tilde{t}}{\int_{-\frac{\tilde{T}_{max}}{2}}^{+\frac{\tilde{T}_{max}}{2}} c^4_{00,\tilde{x}'}(\tilde{t})d\tilde{t}} \tag{9}$$

where $\tilde{t}_0$ (Eq. (6)) is the non-dimensional time instant where $c_{00,\tilde{x}'}(\tilde{t})$ is maximum (Roncallo et al., 2022), $\tilde{S}_{\tilde{v}'}(\tilde{n}) = n_0 S_{\tilde{v}'}(\tilde{n})$ (Eq. (8)). Furthermore, in Eqs. (6), (7) and (9) $c_{00,\tilde{x}'}(\tilde{t})$ and $c_{11,\tilde{x}'}(\tilde{t})$ are the non-dimensional Non-Geometrical Spectral Moments (NGSMs) of the non-dimensional fluctuating part of the response:

$$c_{00,\tilde{x}'}(\tilde{t}) = (2I_v)^2\int_0^{+\infty} |\tilde{Z}(\tilde{n},\tilde{t})|^2\tilde{S}_{\tilde{v}'}(\tilde{n})d\tilde{n} \tag{10}$$

$$c_{11,\tilde{x}'}(\tilde{t}) = (2I_v)^2\int_0^{+\infty} |\dot{\tilde{Z}}(\tilde{n},\tilde{t})|^2\tilde{S}_{\tilde{v}'}(\tilde{n})d\tilde{n} \tag{11}$$

where $\tilde{Z}(\tilde{n},\tilde{t})$ is the non-dimensional Evolutionary Frequency Response Function (EFRF) defined as:

$$\tilde{Z}(\tilde{n},\tilde{t}) = \int_{-\frac{\tilde{T}_{max}}{2}}^{\tilde{t}} \tilde{h}(\tilde{t}-\tilde{\tau})e^{-i2\pi\tilde{n}(\tilde{t}-\tilde{\tau})}\gamma^2(\tilde{\tau})d\tilde{\tau} \tag{12}$$

with $\tilde{h}(\tilde{t})$ the dimensionless impulse response function:

$$\tilde{h}(\tilde{t}) = \frac{1}{2\pi\sqrt{1-\xi^2}}e^{-\xi 2\pi\tilde{t}}\sin\left(2\pi\sqrt{1-\xi^2}\tilde{t}\right)\mathscr{H}(\tilde{t}) \tag{13}$$

being $\mathscr{H}(\tilde{t})$ the Heaviside function.

Furthermore, in Eq. (8) $\tilde{H}(\tilde{n})$ is the non-dimensional complex frequency response function:

$$\tilde{H}(\tilde{n}) = \frac{1}{1-\tilde{n}^2 + 2i\xi\tilde{n}} \tag{14}$$

with i the imaginary unit.

In Eqs. 6–13 the quantities $\tilde{t}$, $\tilde{n}$, $\tilde{T}_{max}$ and $\tilde{x}'$ are non-dimensional parameters defined as follows:

$$\tilde{n} = \frac{n}{n_0};\ \tilde{t} = \frac{t}{T_0};\ \tilde{T}_{max} = \frac{T_{max}}{T_0};\ \tilde{T}_{eq} = \frac{T_{eq}}{T_0};\ \tilde{x}'(t) = \frac{x'(t)}{\bar{x}_{max}} \tag{15}$$

being T_{eq} the equivalent period and x' the fluctuating part of the displacement.

Following the Simplified method defined in Roncallo et al. (2022), which corresponds to the assumption of long pulse duration by Kwon and Kareem (2019, 2009), Eqs. (7) and (9) take the following form:

$$\widetilde{T}_{eq,\gamma} = \int_{-\frac{\widetilde{T}_{max}}{2}}^{+\frac{\widetilde{T}_{max}}{2}} \exp\left[4 - \frac{4\,\mathscr{C}_{\gamma}^{2}}{\gamma^{4}(\widetilde{t})}\right] d\widetilde{t} \tag{16}$$

$$\mathscr{C}_{\gamma}^{2} = \frac{\int_{-\frac{\widetilde{T}_{max}}{2}}^{+\frac{\widetilde{T}_{max}}{2}} \left[\gamma^{4}(\widetilde{t})\right]^{5} d\widetilde{t}}{\int_{-\frac{\widetilde{T}_{max}}{2}}^{+\frac{\widetilde{T}_{max}}{2}} \left[\gamma^{4}(\widetilde{t})\right]^{4} d\widetilde{t}} \tag{17}$$

From Eqs. (16) and (17) it can be deduced that in this particular case the equivalent parameters depend solely on the modulating function $\gamma(\widetilde{t})$ and not on the mechanical properties of the system.

The estimate of the equivalent parameters (Eq. (7) and (9)) and hence of the gust response factor (Eq. (5)) is strictly related to the modulating function of the slowly-varying mean wind speed $\gamma(t)$ and its modelling. This aspect constitutes the major difference in the evaluation of the gust response factor for thunderstorm winds compared to synoptic ones.

2.2. Modulating functions models

In the literature, different models for the modulating function $\gamma(t)$ of the slowly-varying mean wind speed of thunderstorm outflows have been proposed (e.g. Abd-Elaal et al., 2013; Chay et al., 2006; Holmes and Oliver, 2000; Kwon and Kareem, 2009; Ponte and Riera, 2010), which are often based on few or even on a single thunderstorm record. Recently, Roncallo and Solari (2020) proposed two models based on a large number of real-scale records of thunderstorm outflows:

$$\gamma(t) = \frac{1-\gamma^{*}}{\left[1+\left(\frac{t}{T}\right)^{2}\right]^{\frac{1}{2}}} + \gamma^{*} \quad Model\ (I) \tag{18}$$

$$\gamma(t) = (1-\gamma^{*})\exp\left\{-\left(\frac{t}{T}\right)^{2}\right\} + \gamma^{*} \quad Model\ (II) \tag{19}$$

where the parameters γ^{*} and T are, respectively, a measure of the intensity of the background wind speed with respect to the maximum mean wind speed of the thunderstorm outflow, i.e. the mean wind speed observed outside the intense phase of the outflow, and a measure of the duration of its intense phase (Roncallo and Solari, 2020), which can be defined as the time interval in which the ramp-up and rump-down of the thunderstorm wind speed occur (Solari et al., 2015a).

Both Eqs. (18) and (19) do not allow the derivation of an analytical solution of the EFRF (Eq. (12)) suitable for reducing the computational burden of the calculation of the equivalent parameters and gust response factor. For this reason, an alternative function is introduced here, similar to the one adopted by Le and Caracoglia (2017), defined as follows:

$$\gamma(t) = \begin{cases} \frac{1-\gamma^{*}}{2}\left[cos\left(\frac{2\pi t}{T}\right)+1\right]+\gamma^{*}, & |t| < \frac{T}{2} \\ \gamma^{*}, & |t| \geq \frac{T}{2} \end{cases} \quad Model\ (III) \tag{20}$$

By adopting the model in Eq. (20) it is possible to derive a closed-form solution for the EFRF as reported in Appendix I. Despite its complicated appearance, this solution can be easily implemented in numerical programs, drastically reducing the computational time required for the numerical estimate of the EFRF.

It is worth noticing that, in principle, the parameters γ^{*} and T are bounded between 0 and 1 and 0 and T_{max} respectively. However, it is clear that the case $\gamma^{*} = 0$ and $T = 0$ s describes an unrealistic scenario, where the downburst is occurring in absolute absence of background wind and the duration of the intense phase is so short that is instantaneous. Instead, the case $\gamma^{*} = 1$ describes exactly the synoptic event in which there is no modulation in the slowly-varying mean wind speed (and in the turbulence) but it is constant within 10 min, hence returning to the stationary case.

2.2.1. Mean trend of the modulating functions

The modulating functions in Eqs. 18–20 are strictly related to the choice of the couple of parameters γ^{*} and T. In a previous study, Roncallo and Solari (2020) outlined the trends of these parameters on varying the confidence levels of the ensemble of the modulating function records extracted from 129 thunderstorm time histories by means of a moving average technique over 30 s. The records were collected in full-scale in four different ports in the High Tyrrenian sea, i.e. Genoa, La Spezia, Savona and Livorno (Roncallo and Solari, 2020; Solari et al., 2012; Zhang et al., 2018). Starting from the same database, a statistical analysis on the parameters γ^{*} and T is carried out in this study. The values of the couple of parameters γ^{*} and T are investigated by fitting the mean trend of the 129 modulating function $\gamma(t)$, extracted from the thunderstorm records (Romanic et al., 2020; Roncallo and Solari, 2020), employing the models in Eqs. 18–20.

Fig. 1 plots the fitting performed by the three models in Eqs. 18–20 and the ensemble trend of the functions $\gamma(t)$ extracted from the data. Table 1 reports the parameters γ^{*} and T corresponding to the fitting in Fig. 1.

Fig. 1 shows that model I furnishes an accurate representation of the mean trend while models II and III are more approximated ones. Moreover, it can be observed that while the values assumed by the parameter γ^{*} are similar for the three models, the parameter T related to model III results significantly greater than the ones from models I and II. Indeed, although it retains the same physical meaning within all the three models in Eqs. 18–20, in the case of Eq. (20), according to the analytical model of the function in piecewise form, it specifies the duration of the interval in which $\gamma(t) \geq \gamma^{*}$.

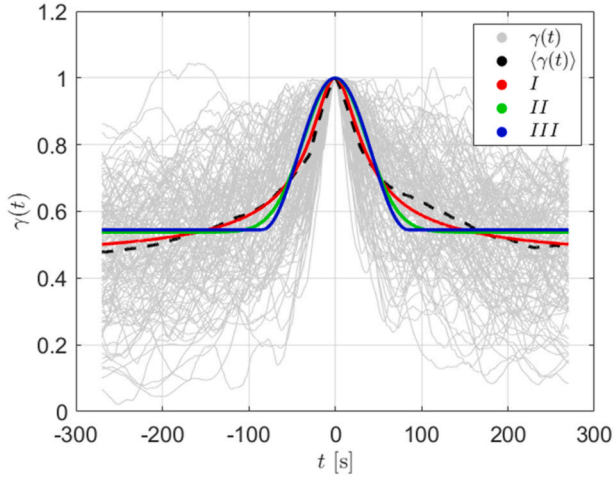

Fig. 1. Comparison of the models of the modulating function γ: Eq. (18) model I; Eq. (19) model II; Eq. (20) model III.

Table 1
Parameters γ^{*} and T extracted by fitting the mean trend of the function $\gamma(t)$ with models I, II and III.

Model	I (Eq. (18))	II (Eq. (19))	III (Eq. (20))
γ^{*}	0.447	0.538	0.545
T [s]	26.459	51.344	169.805

For sake of completeness, the same analyses were carried out port by port in order to investigate the possible differences between the thunderstorms collected in different locations and results are very similar to the ones obtained from the whole database. Therefore, it was concluded that no significant advantages are provided by carrying out separated analysis per each location and only results for the complete database are reported here. However, it is worth noticing that the locations considered are coastal areas and thus similar from an orographic point of view. Different values of the parameters γ^* and T may be found in regions characterized by a different morphology.

2.2.2. Variability of the parameters

In view of the differences between the wind speed records produced by one thunderstorm and another, the trends of the modulating functions of the associated slowly-varying mean wind speed may be, in general, different, as shown by the ensemble in Fig. 1. Therefore, different values of the parameters γ^* and T provide the best fit to each sample function.

For this reason, an analysis on the range of variation of the quantities γ^* and T is carried out, starting from the estimate of the parameters from each of the 129 records of the modulating function. As an example, Fig. 2 shows two samples of the modulating function extracted from the database fitted by the three analytical models.

It is observed that, differently from the mean trends previously discussed, models II and III (Eqs. 19 and 20) give a better fitting of the peak, especially when the duration of the intense phase is shorter (Fig. 2b). Instead, when the peak is sharper (Fig. 2a), model I gives a better representation compared to models II and III. Moreover, the regions outside the peak are well represented by all the three models. Although the models provide overall good fits of the samples available, in few cases they were not able to properly represent the functions extracted from the data. In these cases the obtained parameters γ^* and T where considered not reliable and were not included in the analyses. Figs. 3–5 plot the couples of the parameters γ^* and T obtained from the fittings by the three analytical models along with their estimated pdfs.

From Figs. 3b–5b it can be observed that no particular trends are detected for the parameters γ^* and T, being distributed like a cloud especially for models II and III (Figs. 4b and 5b). This is confirmed by Table 2, reporting the correlation coefficient $\rho_{\gamma^*,T}$ between γ^* and T, showing a weak correlation between the two parameters for all the three models.

By fixing the levels of non-exceeding probability of 10% and 90%, a representative range of variability of the parameters γ^* and T can be defined, which is reported in Table 3 for the three models in Eqs. 18–20 along with their mean value and the coefficient of variation (c.o.v).

Overall, these results are in accordance with the values derived from the mean trend of the modulating function $\gamma(t)$ in Table 1. Moreover, observing the values of the c.o.v. of the two parameters, it can be deduced that the parameter T results quite dispersed if compared with γ^*. It is worth to notice that, although the parameter T is proportional to the duration of the intense phase of the outflow, its definition is a delicate aspect (Solari et al., 2015a). In view of the different analytical expression of the models, different values of the parameter T associated to different models can correspond to the same duration of the intense phase.

3. Gust factor sensitivity to the modulating function

In this Section, the sensitivity of the gust response factor to the analytical model adopted for the modulating function $\gamma(t)$ is studied by comparing Eq. (5), evaluated for a set of SDOF systems with $n_0 \in [0.05, 3]$ Hz and $\xi \in [0.2\%, 5\%]$, employing the three models in Eqs. 18–20 and setting the couples of parameters γ^* and T in order to best trace the mean trend of the modulating function $\gamma(t)$ (Section 2.2.1, Table 1).

The comparison between the gust response factors evaluated employing the three models of the function $\gamma(t)$ is reported in Fig. 6, following the Rigorous (Eq. (7) and (9), Fig. 6a) and Simplified method (Eq. (16) and (17), Fig. 6b), respectively.

Fig. 6 shows that models II and III (Eqs. 19 and 20) furnish identical values of the gust response factor for both the Rigorous and Simplified methods, as expected in view of the similarity between the two modulating functions. However, models II and III (Eq. (19) and (20)) give values of the gust response factor slightly higher than the ones furnished by model I (Eq. (18)), especially for lowly-damped systems. However, Fig. 6 shows that the gust response factor is not much affected by the shape of the modulating function, being the differences between the gust response factor evaluated employing a model or another not so significant. This is an important result since it allows to adopt only one model among the three proposed to carry out the study without affecting the results from both a qualitative and quantitative point of view, provided that the parameters γ^* and T are properly fixed. Therefore, since for model III an analytical solution for the EFRF is derived (Appendix I) which drastically reduces the computational burden of the gust response factor evaluation, the next analyses are carried out assuming model III (Eq. (20)) for $\gamma(t)$.

4. General tendencies of the equivalent parameters

In this Section the general tendencies of the equivalent parameters $\mathscr{C}$ and $\widetilde{T}_{eq}$ with γ^* and T are portrayed and discussed. The analyses are

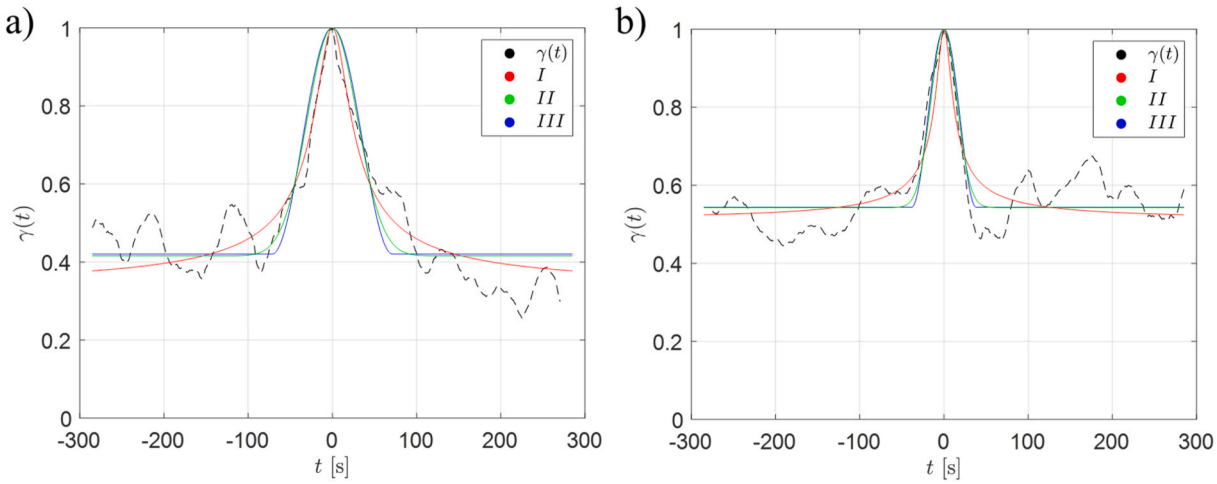

Fig. 2. Samples of the modulating function extracted from the database fitted by the analytical models in Eqs. 18–20.

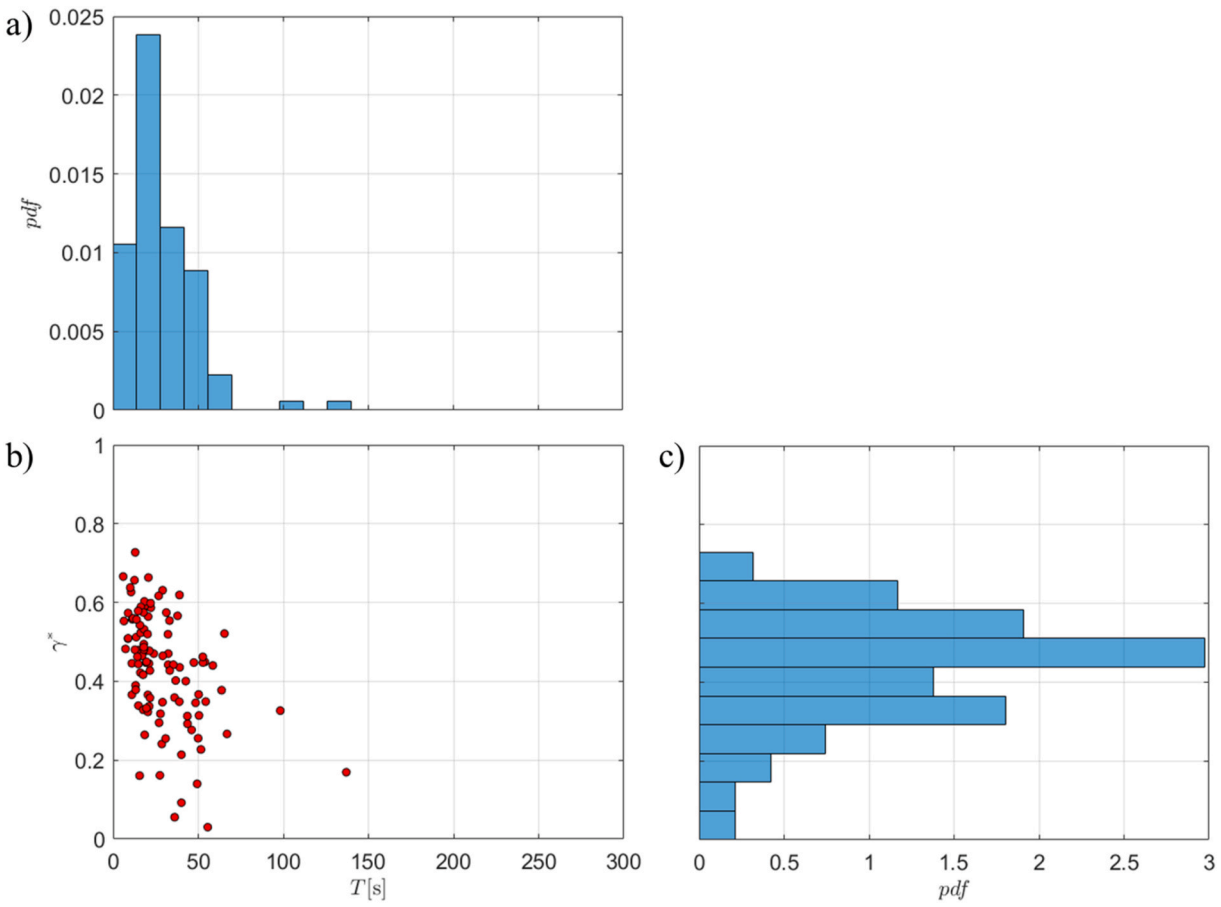

Fig. 3. Values of the parameters γ^* and T extracted from the time-histories employing model I in Eq. (18): (a) pdf of T; (b) couples of γ^* and T extracted from each time-history; (c) pdf of γ^*.

carried out employing model III, introducing the following non-dimensional quantities:

$$\widetilde{T} = \frac{T}{T_0}; \ \mathscr{T} = \frac{T}{T_{max}} \tag{21}$$

where $\widetilde{T}$ is duration of the intense phase of the outflow normalized with the fundamental period of the structure and plays the role of a non-dimensional fundamental frequency whereas $\mathscr{T}$ is the duration of the intense phase with respect to the whole duration of the phenomenon T_{max}. According to the definition in Eq. (15), it follows that $\widetilde{T}_{max} = T_{max}/T_0 = \widetilde{T}/\mathscr{T}$. It is important to point out that, while $\mathscr{T}$ is strictly a property of the wind speed of the thunderstorm, $\widetilde{T}$ relates the duration of the intense phase of the thunderstorm with a mechanical property of the dynamical system.

At first, the equivalent parameters obtained for the Simplified method are portrayed. Fig. 7 plots the parameters $\mathscr{C}^2_\gamma$ and $\widetilde{T}_{eq,\gamma}$ (Eqs. 16 and 17), this latter normalized with $\widetilde{T}_{max}$, as functions of γ^* and for different values of $\mathscr{T} = [1/6, 1/4, 1/2]$ in accordance with the results reported for the parameter T in Table 3.

It can be observed that the dependence of $\mathscr{C}^2_\gamma$ on $\mathscr{T}$ becomes more relevant in a neighbourhood of $\gamma^* = 0.85$ (Fig. 7a). Instead, $\widetilde{T}_{eq,\gamma}$ (Fig. 7b) shows a more significant dependence on $\mathscr{T}$ when $\gamma^* \leq 0.8$. It is important to notice that for $\gamma^* \to 1$ the parameter $\mathscr{C}^2_\gamma$ collapses to unity while $\widetilde{T}_{eq,\gamma} \to \widetilde{T}_{max}$, leading to the case of a stationary wind. Moreover, it can be observed that $\mathscr{C}^2_\gamma \leq 1$ and $\widetilde{T}_{eq,\gamma} \leq \widetilde{T}_{max}$ for all values of γ^*. These results highlight how, due to the presence of the modulating function – i.e. the non-stationarity – of the loading, the standard deviation of the alongwind response results lower than the one of the stationary case ($\mathscr{C}^2_\gamma = 1$). At the same time, the temporal interval over which the maximum value of the response is expected is significantly reduced. Indeed, for $\gamma^* \leq 0.8$ the parameter $\widetilde{T}_{eq,\gamma}$ shows more than the 70% of reduction compared to $\widetilde{T}_{max}$. These behaviours are more pronounced the more $\mathscr{T}$ decreases.

When the rigorous formulation is adopted, the non-dimensional equivalent parameters $\mathscr{C}^2$ and $\widetilde{T}_{eq}$ (Eq. (7) and (9)) are also function of the mechanical properties of the system, i.e. damping ratio ξ and $\widetilde{T}$ (Eq. (21)). Fig. 8 plots the trends of the parameters $\mathscr{C}^2$ and $\widetilde{T}_{eq}$ (red solid lines) for different values of $\widetilde{T}$ and ξ and for a fixed value of $\mathscr{T} = 1/4$, along with the corresponding parameters $\mathscr{C}^2_\gamma$ and $\widetilde{T}_{eq,\gamma}$ from the Simplified method (black dashed lines) for comparison.

It can be observed that $\mathscr{C}^2_\gamma$ and $\widetilde{T}_{eq,\gamma}$ are, respectively, an upper and lower bound for $\mathscr{C}^2$ and $\widetilde{T}_{eq}$ that are reached for high values of $\widetilde{T}$ and ξ (Fig. 8e and f). For lower values of $\widetilde{T}$ and ξ (Fig. 8a and b) the tendencies of both the parameters $\mathscr{C}^2$ and $\widetilde{T}_{eq}$ change significantly with respect to the ones estimated adopting the simplified formulation.

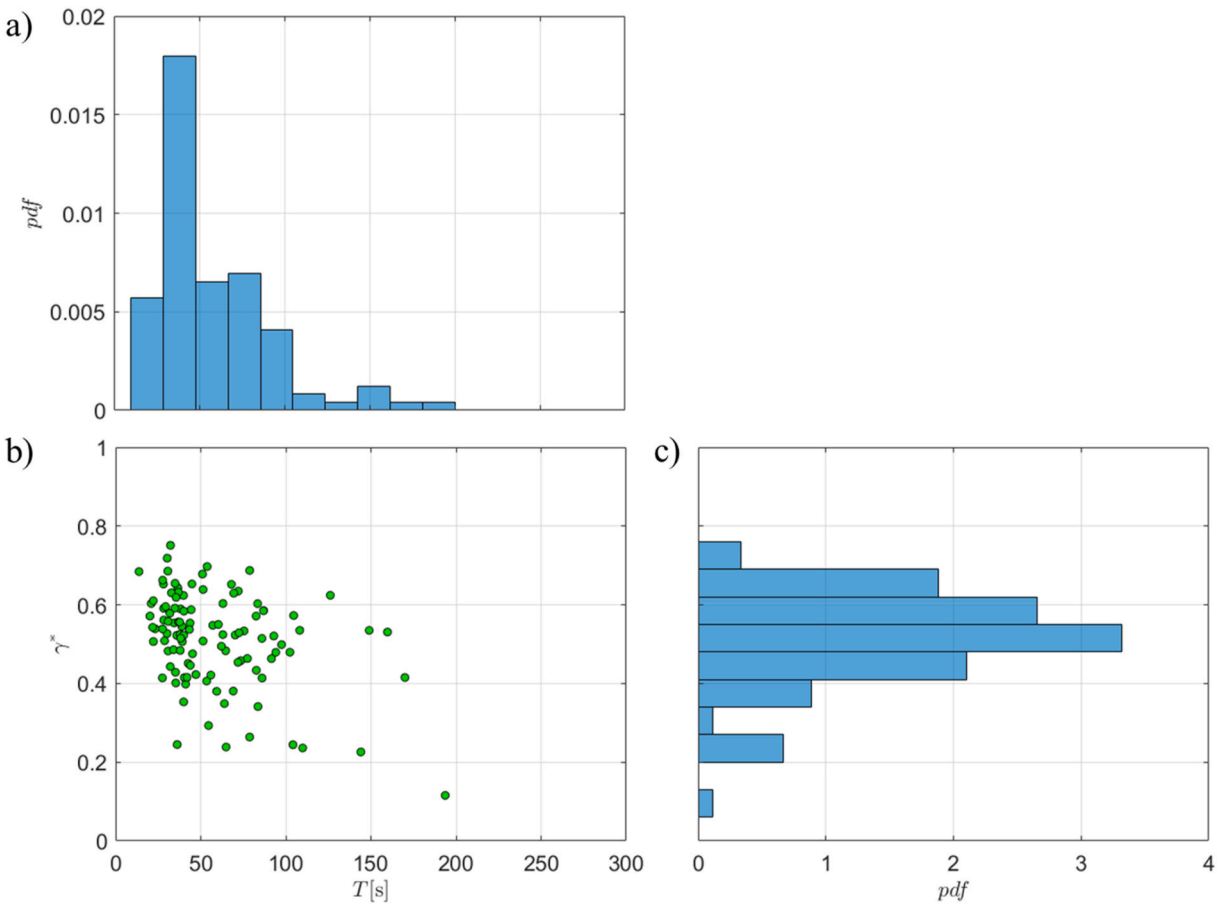

Fig. 4. Values of the parameters γ^* and T extracted from the time-histories employing model II in Eq. (19): (a) pdf of T; (b) couples of γ^* and T extracted from each time-history; (c) pdf of γ^*.

These tendencies have a physical interpretation. When $\widetilde{T}$ is high (Fig. 8e and f), the dynamic effects of the modulating function are negligible, instead when $\widetilde{T}$ is low (Fig. 8c and d), they are dominant and reduce the variance of the response. Moreover, when $\widetilde{T}$ is very low (Fig. 8a and b) it means that the duration of the intense phase of the thunderstorm is extremely short compared with the fundamental period and hence the non-stationarity of the loading is not perceived by the structure. In this limit case the modulating function collapses to γ^{*4} and, as a result (Fig. 8a) $\mathscr{C}^2 \rightarrow \gamma^{*4}$, consequently it is reasonable to expect that $\widetilde{T}_{eq}/\widetilde{T}_{max} \rightarrow 1$. This can be demonstrated by substituting $\mathscr{C}^2 = \gamma^{*4}$ and $c_{00,\bar{x}'}(\tilde{t}) = (2\bar{I}_v)^2 \widetilde{J}^2 \gamma^{*4}$ in Eq. (7).

5. Gust response factor sensitivity to the modulating function parameters

In this Section, a sensitivity analysis is carried out directly focusing on the gust response factor by varying the parameters γ^* and $\mathscr{T}$, aiming to investigate how the effects outlined in Section 4 on the equivalent parameters play out when combined together. Therefore, according to the results reported in Table 3, the values $\gamma^* = [0.3, 0.5, 0.7]$ and $\mathscr{T} = [1/6, 1/4, 1/2]$ are considered in this analysis.

Fig. 9 plots the tendencies of the gust response factor evaluated with both the Simplified and Rigorous method (dashed and solid lines, respectively), for different fundamental frequencies and damping ratios, varying the parameters γ^* and $\mathscr{T}$. In particular Fig. 9a,c and e plot the tendencies of the gust response factor fixing the parameter $\gamma^* = 0.5$ and varying $\mathscr{T}$ whilst Fig. 9b,d and f plot the same tendencies fixing $\mathscr{T} = 1/4$ and varying γ^*.

Firstly, it can be observed that, for all the damping ratios and following either the Rigorous or the Simplified method, on increasing γ^* or $\mathscr{T}$ the gust response factor increases. Moreover, the variations due to both γ^* and $\mathscr{T}$ are more significant when the damping ratio and the fundamental frequency are low (Fig. 9a and b), while for highly damped and stiffer systems the role of the two parameters is negligible (Fig. 9e and f).

Another important aspect is the different behaviour portrayed for the Rigorous and Simplified method. When adopting the Simplified method, the variation of the gust response factor with both $\mathscr{T}$ and γ^* is regular, with the curves that remain very similar from a qualitative point of view. Moreover, it can be observed that the gust response factor estimated with the Simplified method is not so sensitive to the parameter γ^* also for the case of lowly-damped and flexible systems while it is more sensible to the variation of $\mathscr{T}$ as pointed out in Fig. 9a and b. On the other hand, the tendencies portrayed by the Rigorous method are more affected by the variation of the parameters γ^* and $\mathscr{T}$. As an example, it can be observed in Fig. 9a and b how for a system with $n_0 = 0.2$ Hz the gust response factor shows a increase of about 34% (Figs. 9a) and 37% (Fig. 9b) moving from $\mathscr{T} = 1/6$ to $\mathscr{T} = 1/2$ and $\gamma^* = 0.3$ to $\gamma^* = 0.7$ respectively. Moreover, the maximum of G_x moves towards the region of lower fundamental frequencies by increasing γ^* or $\mathscr{T}$, tending to the

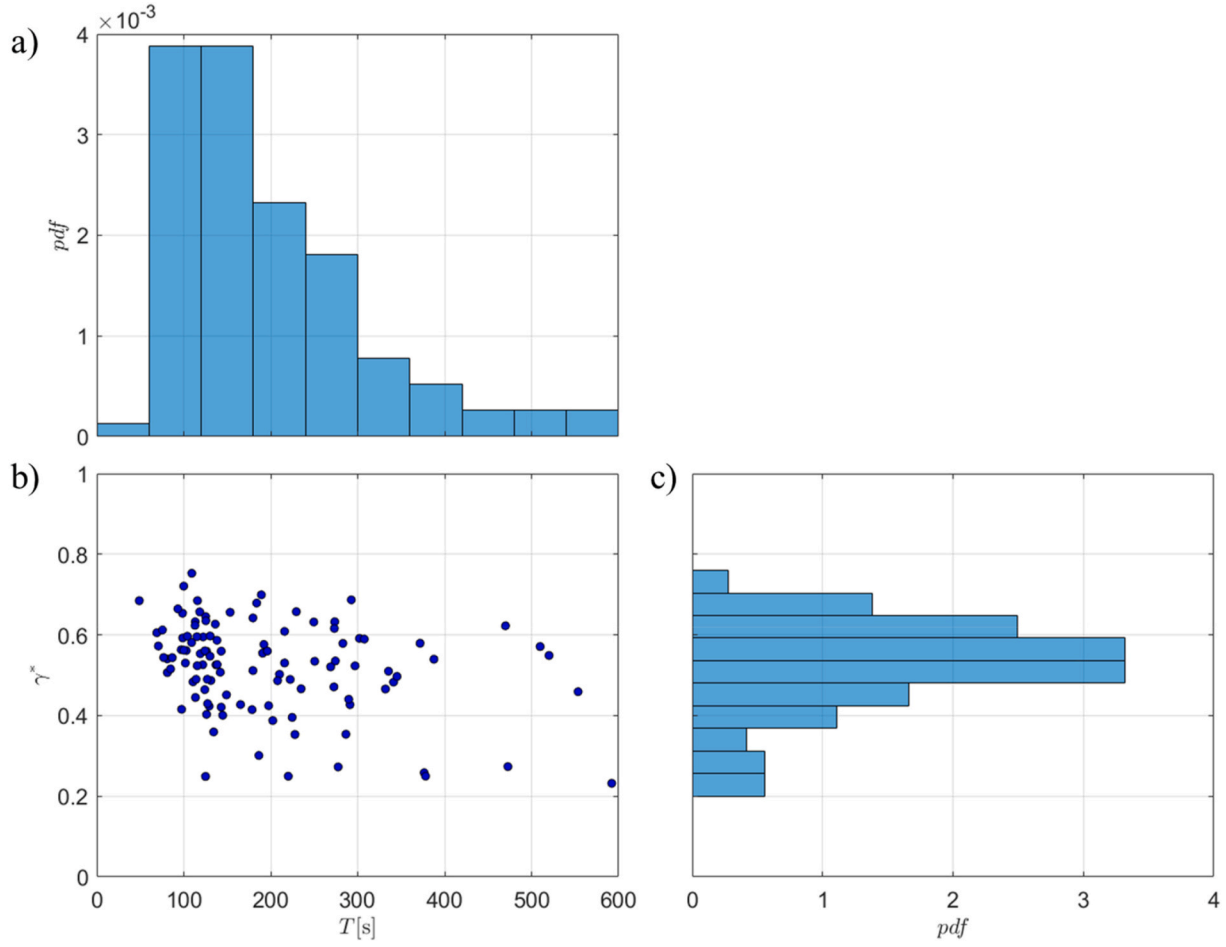

Fig. 5. Values of the parameters γ^* and T extracted from the time-histories employing model III in Eq. (20): (a) pdf of T; (b) couples of γ^* and T extracted from each time-history; (c) pdf of γ^*.

Table 2
Correlation coefficient $\rho_{\gamma^*,T}$ between γ^* and T.

Model	I	II	III
$\rho_{\gamma^*,T}$	−0.465	−0.383	−0.309

Table 3
Range of variability of the parameters γ^* and T levels of non-exceeding probability of 90% and 10%; mean values $\langle\gamma^*\rangle$ and $\langle T\rangle$ and coefficient of variation (c.o.v).

Model	I	II	III
γ^*	0.25–0.60	0.36–0.65	0.37–0.65
$\langle\gamma^*\rangle$	0.432	0.514	0.522
$c.o.v.(\gamma^*)$	0.326	0.230	0.215
T [s]	11.24–52.66	28.15–100.45	97.22–343.59
$\langle T\rangle$ [s]	28.940	57.960	196.463
$c.o.v.(T)$	0.679	0.583	0.579

curves related to the Simplified method. This is due to the fact that by increasing γ^* or $\mathscr{T}$ the loading condition tends to be stationary, inhibiting the dynamic effects due to the modulating function. In these circumstances, the adoption of the Simplified method becomes more reliable since the two methods furnish almost the same values of gust response factor. It is worth noticing that for $\gamma^* = 1$ – i.e. stationary wind with $\gamma(t) = 1$ (Eqs. 18–20) – the gust response factor from Davenport (1967) is found as a particular case.

On the basis of these results two main aspects are worth to be mentioned. Firstly, the variation of the two parameters γ^* and $\mathscr{T}$ is, in general, non-negligible for an accurate estimation of the gust response factor due to thunderstorm outflows, therefore their role needs to be accounted in the derivation of the equivalent parameters. It can be neglected only when the system is stiff and highly damped. Secondly, it can be deduced that assuming $\gamma^* = 0$ (i.e. neglecting the role of the background wind as proposed by other models in literature) leads to lower values of the gust response factor and hence it may not be conservative from a design perspective. This assumption may be reliable for the Simplified method since in that case the gust response factor is not that affected by the variation of γ^*. Nevertheless, such approach becomes overconservative when the system is flexible and lowly-damped (Fig. 9a and b) (Roncallo et al., 2022).

6. Final remarks and some prospects

The present study investigated the tendencies and sensitivity of the thunderstorm gust response factor to the analytical model adopted for the modulating function of the slowly-varying mean wind speed and its characteristic parameters, according to the EPSD model developed by Roncallo and Solari (2020).

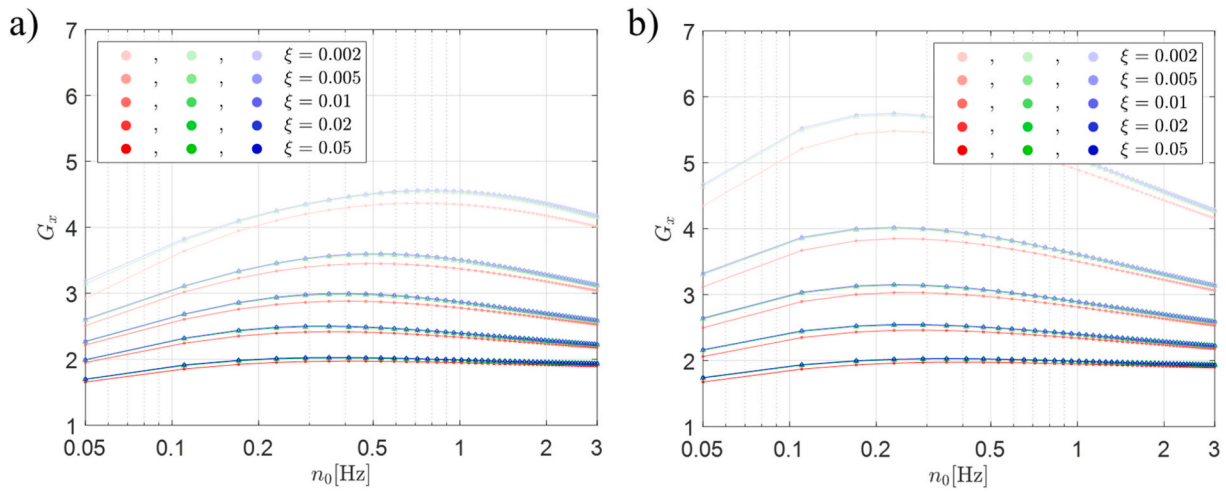

Fig. 6. Gust factor of the dynamic response derived employing model I (Eq. (18) red lines), model II (Eq. (19) green lines) and model III (Eq (20) blue lines): Rigorous method (a); Simplified method (b).

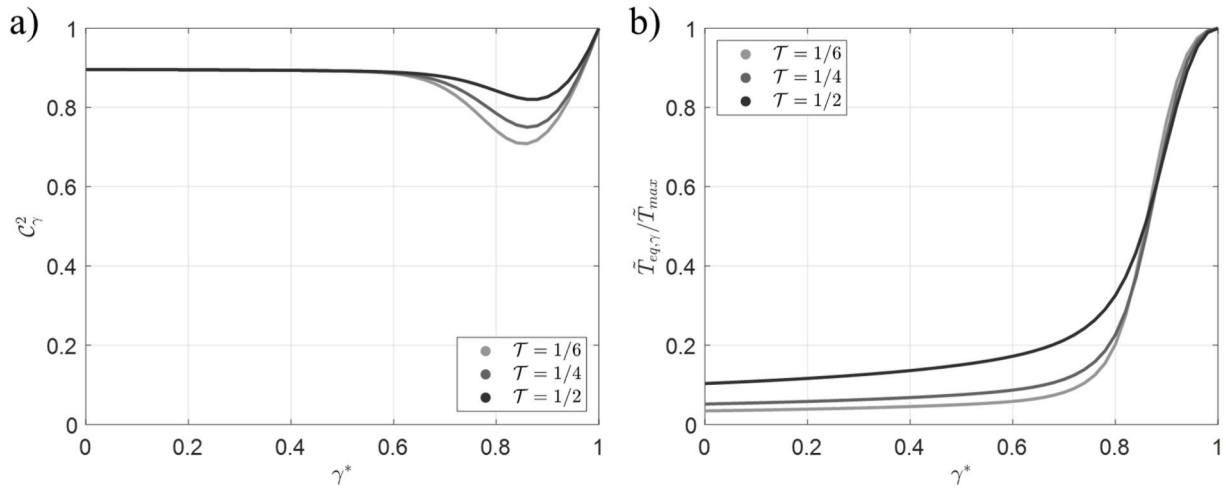

Fig. 7. Trends of the parameters $\mathscr{C}_\gamma^2$ and $\widetilde{T}_{eq,\gamma}$ versus γ^* for different values of $\mathscr{T}$.

The statistical analysis carried out has shown, on the one hand, a negligible correlation between the parameters of the modulating function models and, on the other hand, a significant variation of these quantities. Therefore, a suitable range of variation has been defined for both the background wind speed and the duration of the intense phase of the thunderstorm outflow.

The sensitivity of the gust response factor to the modulating function of the wind speed has shown that very similar trends are obtained employing the different models proposed. In light of this result, for the successive analysis a newly proposed model, called model III, has been adopted, which allows for an analytical solution of the EFRF, that has been derived and employed in the sensitivity analysis to reduce the computational burden.

The analysis pointed out that the gust response factor is sensitive to the variation of the two parameters of the modulating function. In particular, the gust response factor increases by increasing the background wind or the duration of the intense phase. Furthermore, the gust response factor evaluated with the Rigorous method tends to the one derived with the Simplified method (i.e. neglecting the transient dynamic effects) when the structure is highly damped and stiff and on increasing the two parameters of the modulating function. These results proved that the choice of the two parameters becomes more delicate the more the structure is lowly damped and flexible. Moreover, it has been observed that the gust response factor for stationary winds figures as a particular case of the generalized formulation proposed for thunderstorm outflows.

In view of the obtained results, the role of the two parameters of the slowly-varying mean wind speed, along with the transient dynamic effects, cannot be neglected especially for flexible and lowly-damped systems.

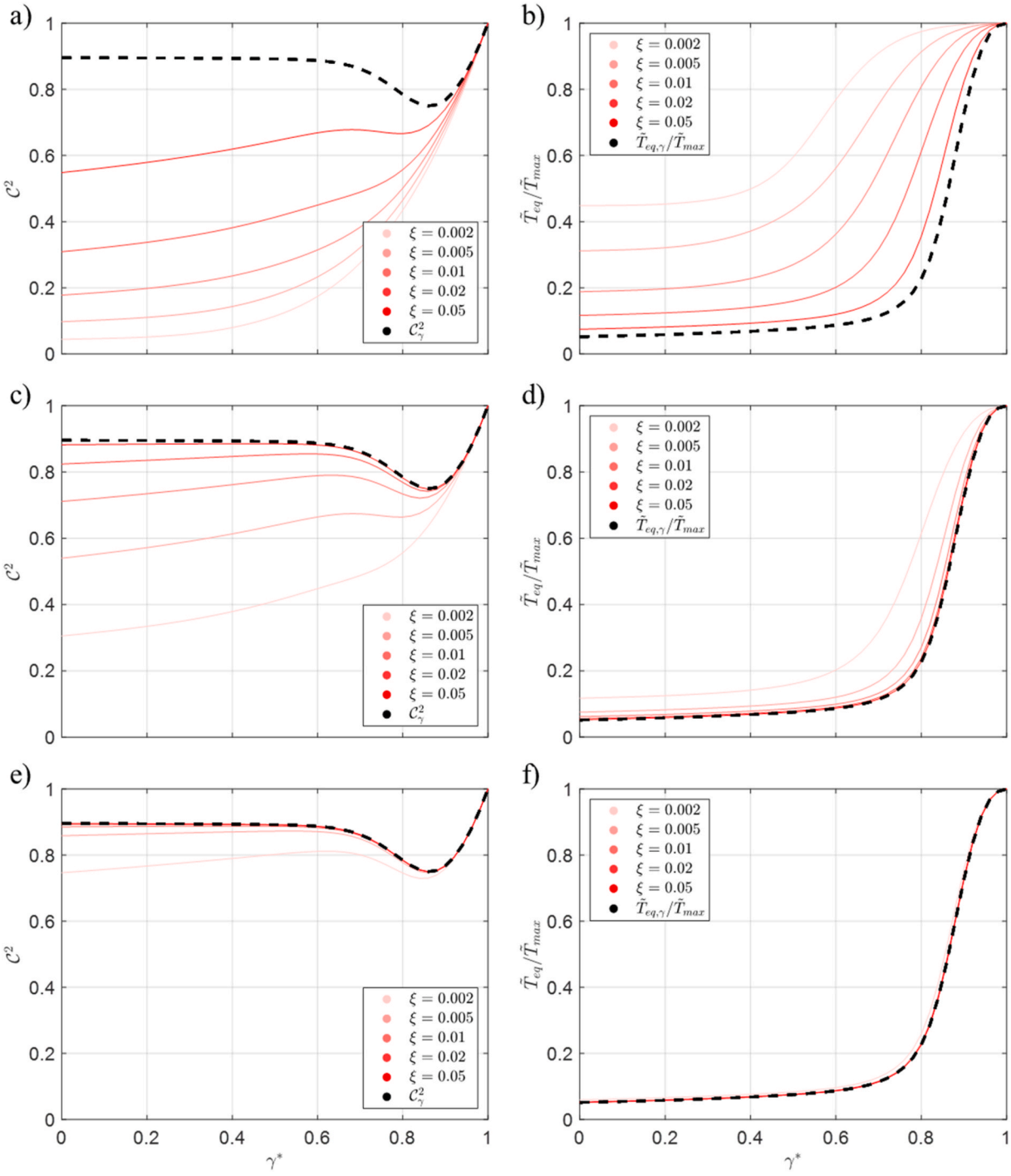

Fig. 8. Trends of the parameters $\mathscr{C}^2$ and $\widetilde{T}_{eq}$ for different values of $\widetilde{T}$ and damping ratio ξ ($\mathscr{T} = 1/4$): a,b) $\widetilde{T} = 7.5$; c,d) $\widetilde{T} = 75$; e,f) $\widetilde{T} = 450$.

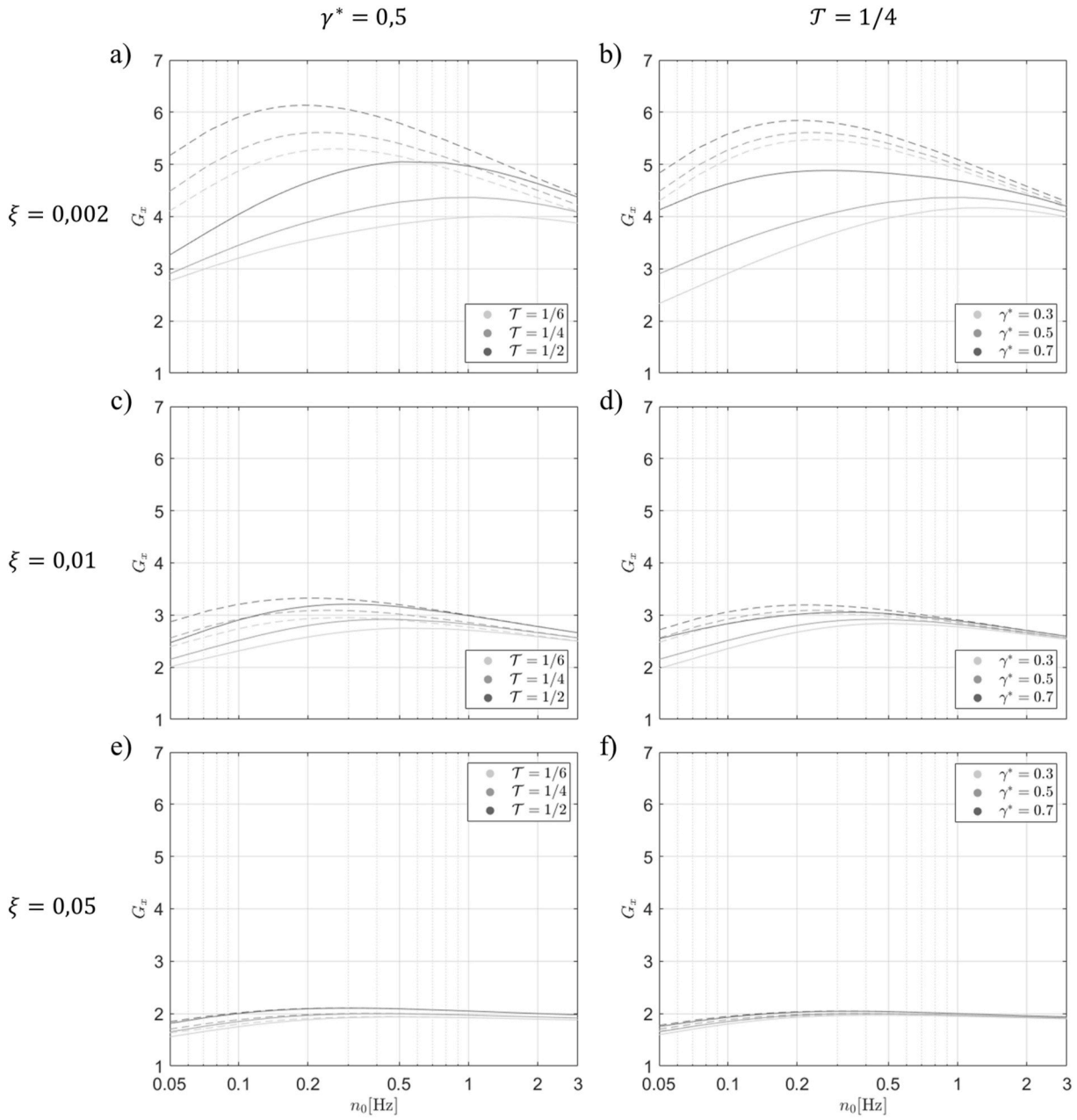

Fig. 9. Sensitivity analysis of the gust factor (Solid line for the Rigorous method, dashed lines for the Simplified method): (a,c,e) $\gamma^* = 0.5$; (b,d,f) $\mathcal{T} = 1/4$; (a,b) $\xi = 0.2\%$, (c,d) $\xi = 1\%$, (e,f) $\xi = 5\%$.

Despite the availability of a closed-form solution for the EFRF, the generalized gust response factor based on the proposed formulation can be estimated only numerically. In order to simplify its derivation for practical engineering calculations it is advisable to search approximated closed-form solutions able to account for the transient dynamic effects, the role of the background wind and duration of the intense phase of the outflow.

CRediT authorship contribution statement

Luca Roncallo: Conceptualization, Methodology, Software, Validation, Formal analysis, Investigation, Data curation, Writing – original draft, Visualization. **Federica Tubino:** Conceptualization, Methodology, Supervision, Writing – review & editing.

Declaration of competing interest

The authors declare that they have no known competing financial interests or personal relationships that could have appeared to influence the work reported in this paper.

Data availability

Data will be made available on request.

Acknowledgements

This research is funded by the European Research Council (ERC) under the European Union's Horizon 2020 research and innovation program (grant agreement No. 741273) for the project THUNDERR -

Detection, simulation, modelling and loading of thunderstorm outflows to design wind-safer and cost-efficient structures - supported by an Advanced Grant 2016.

The data used for this research was recorded by the monitoring network set up as part of the European Projects Winds and Ports (grant No. B87E09000000007) and Wind, Ports and Sea (grant No. B82F13000100005), funded by the European Territorial Cooperation Objective, Cross-border program Italy-France Maritime 2007–2013.

The authors are deeply grateful to Prof. Giovanni Solari for his essential input and motivation for this research within the project THUNDERR.

Appendix I. A Closed-Form solution for the Evolutionary Frequency Response Function

A closed-form solution for the EFRF (Eq. (12)) is proposed using the model for the modulating function $\gamma(t)$ in Eq. (20). The solution is searched in non-dimensional form using the dimensionless parameters defined in Eqs. (15) and (21).

Starting from the definition of the EFRF in Eq. (12), the lower integration limit can be extended to $-\infty$ by imposing $\widetilde{T}_{max} \to +\infty$ as follows:

$$\widetilde{Z}(\widetilde{n},\widetilde{t}) = \int_{-\infty}^{\widetilde{t}} \widetilde{h}(\widetilde{t}-\widetilde{\tau}) e^{-i2\pi\widetilde{n}(\widetilde{t}-\widetilde{\tau})} \gamma^2(\widetilde{\tau}) d\widetilde{\tau} \tag{22}$$

Substituting Eq. (20) in Eq. (22), after very simple algebra, it leads to the following conditional non-dimensional function:

$$\widetilde{Z}(\widetilde{n},\widetilde{t}) = \begin{cases} \gamma^{*2} \displaystyle\int_{-\infty}^{\widetilde{t}} \widetilde{h}(\widetilde{t}-\widetilde{\tau}) e^{-i2\pi\widetilde{n}(\widetilde{t}-\widetilde{\tau})} d\widetilde{\tau}, & \widetilde{t} < -\dfrac{\widetilde{T}}{2} \\ \gamma^{*2} \displaystyle\int_{-\frac{\widetilde{T}}{2}}^{\widetilde{t}} \widetilde{h}(\widetilde{t}-\widetilde{\tau}) e^{-i2\pi\widetilde{n}(\widetilde{t}-\widetilde{\tau})} d\widetilde{\tau} + \int_{-\frac{\widetilde{T}}{2}}^{\widetilde{t}} \widetilde{h}(\widetilde{t}-\widetilde{\tau}) e^{-i2\pi\widetilde{n}(\widetilde{t}-\widetilde{\tau})} \gamma_c(\widetilde{\tau}) d\widetilde{\tau}, & -\dfrac{\widetilde{T}}{2} \le \widetilde{t} \le \dfrac{\widetilde{T}}{2} \\ \displaystyle\int_{-\frac{\widetilde{T}}{2}}^{\frac{\widetilde{T}}{2}} \widetilde{h}(\widetilde{t}-\widetilde{\tau}) e^{-i2\pi\widetilde{n}(\widetilde{t}-\widetilde{\tau})} \gamma_c(\widetilde{\tau}) d\widetilde{\tau} + \gamma^{*2} \int_{\frac{\widetilde{T}}{2}}^{+\infty} \widetilde{h}(\widetilde{t}-\widetilde{\tau}) e^{-i2\pi\widetilde{n}(\widetilde{t}-\widetilde{\tau})} d\widetilde{\tau}, & \widetilde{t} > \dfrac{\widetilde{T}}{2} \end{cases} \tag{23}$$

where:

$$\gamma_c(\widetilde{\tau}) = \left\{ \frac{1-\gamma^*}{2} \left[cos\left(\frac{2\pi\widetilde{\tau}}{\widetilde{T}} \right) + 1 \right] + \gamma^* \right\}^2 - \gamma^{*2} \tag{24}$$

Eq. (23) can be rewritten as:

$$\widetilde{Z}(\widetilde{n},\widetilde{t}) = \gamma^{*2} \int_{-\infty}^{+\infty} \widetilde{h}(\widetilde{t}-\widetilde{\tau}) e^{-i2\pi\widetilde{n}(\widetilde{t}-\widetilde{\tau})} d\widetilde{\tau} + \begin{cases} 0, & \widetilde{t} < -\dfrac{\widetilde{T}}{2} \\ \displaystyle\int_{-\frac{\widetilde{T}}{2}}^{\widetilde{t}} \widetilde{h}(\widetilde{t}-\widetilde{\tau}) e^{-i2\pi\widetilde{n}(\widetilde{t}-\widetilde{\tau})} \gamma_c(\widetilde{\tau}) d\widetilde{\tau}, & -\dfrac{\widetilde{T}}{2} \le \widetilde{t} \le \dfrac{\widetilde{T}}{2} \\ \displaystyle\int_{-\frac{\widetilde{T}}{2}}^{\frac{\widetilde{T}}{2}} \widetilde{h}(\widetilde{t}-\widetilde{\tau}) e^{-i2\pi\widetilde{n}(\widetilde{t}-\widetilde{\tau})} \gamma_c(\widetilde{\tau}) d\widetilde{\tau}, & \widetilde{t} > \dfrac{\widetilde{T}}{2} \end{cases} \tag{25}$$

where the first integral is the transfer function in Eq. (14). This leads to the following expression for the EFRF:

$$\widetilde{Z}(\widetilde{n},\widetilde{t}) = \gamma^{*2} \widetilde{H}(\widetilde{n}) + \widetilde{Z}_0(\widetilde{n},\widetilde{t}) \tag{26}$$

with:

$$\widetilde{Z}_0(\widetilde{n},\widetilde{t}) = \begin{cases} 0, & \widetilde{t} < -\dfrac{\widetilde{T}}{2} \\ \widetilde{Z}_T(\widetilde{n},\widetilde{t}), & -\dfrac{\widetilde{T}}{2} \le \widetilde{t} \le \dfrac{\widetilde{T}}{2} \\ \widetilde{Z}_r(\widetilde{n},\widetilde{t}), & \widetilde{t} > \dfrac{\widetilde{T}}{2} \end{cases} \tag{27}$$

where, substituting Eq. (24) in Eq. (25), the functions $\widetilde{Z}_T(\widetilde{n},\widetilde{t})$ and $\widetilde{Z}_r(\widetilde{n},\widetilde{t})$ read:

$$\widetilde{Z}_T(\widetilde{n},\widetilde{t}) = \int_{-\frac{\widetilde{T}}{2}}^{\widetilde{t}} \widetilde{h}(\widetilde{t}-\widetilde{\tau}) e^{-i2\pi\widetilde{n}(\widetilde{t}-\widetilde{\tau})} \left\{ \frac{(1-\gamma^*)^2}{4}\left[cos\left(\frac{2\pi\widetilde{\tau}}{\widetilde{T}}\right)+1\right]^2 + \gamma^*(1-\gamma^*)\left[cos\left(\frac{2\pi\widetilde{\tau}}{\widetilde{T}}\right)+1\right]\right\} d\widetilde{\tau} \tag{28}$$

$$\widetilde{Z}_r(\widetilde{n},\widetilde{t}) = \int_{-\frac{\widetilde{T}}{2}}^{\frac{\widetilde{T}}{2}} \widetilde{h}(\widetilde{t}-\widetilde{\tau}) e^{-i2\pi\widetilde{n}(\widetilde{t}-\widetilde{\tau})} \left\{ \frac{(1-\gamma^*)^2}{4}\left[cos\left(\frac{2\pi\widetilde{\tau}}{\widetilde{T}}\right)+1\right]^2 + \gamma^*(1-\gamma^*)\left[cos\left(\frac{2\pi\widetilde{\tau}}{\widetilde{T}}\right)+1\right]\right\} d\widetilde{\tau} \tag{29}$$

The integrals in Eqs. (28) and (29) can be analytically solved and they read:

$$\widetilde{Z}_T(\widetilde{n},\widetilde{t}) = \sum_{j=0}^{4} c_j \widetilde{Z}_{T,j}(\widetilde{n},\widetilde{t}) \tag{30}$$

$$\widetilde{Z}_r(\widetilde{n},\widetilde{t}) = \sum_{j=0}^{4} c_j \widetilde{Z}_{r,j}(\widetilde{n},\widetilde{t}) \tag{31}$$

where:

$$c_j = 2^{-2|j-2|}\left(1-\gamma_*^{3-|j-2|}\right)^{|j-2|} - \delta_{2j}\left[\frac{5}{8}(\gamma^*-1)\left(\gamma^*+\frac{3}{5}\right)+1\right] \tag{32}$$

$$\begin{aligned}\widetilde{Z}_{T,j}(\widetilde{n},\widetilde{t}) = {} & \left(\lambda\pi - 2\pi\widetilde{T}\sqrt{1-\xi^2}\right)\frac{\exp\left[-\pi\widetilde{T}\left(\frac{2\widetilde{t}}{\widetilde{T}}+1\right)(i\widetilde{n}+\xi)\right]\cos\left[\frac{\lambda\pi}{2}-\pi\widetilde{T}\sqrt{1-\xi^2}\left(\frac{2\widetilde{t}}{\widetilde{T}}+1\right)\right]-\cos\left(\frac{\lambda\pi\widetilde{t}}{\widetilde{T}}\right)}{\frac{\sqrt{1-\xi^2}}{2\pi\widetilde{T}}\left(\lambda^2\pi^2-4\lambda\pi^2\widetilde{T}\sqrt{1-\xi^2}+\frac{4\pi^2\widetilde{T}^2}{\widetilde{H}(\widetilde{n})}\right)} \\ & + 2\pi\widetilde{T}(i\widetilde{n}+\xi)\frac{\exp\left[-\pi\widetilde{T}\left(\frac{2\widetilde{t}}{\widetilde{T}}+1\right)(i\widetilde{n}+\xi)\right]\mathrm{sen}\left[\frac{\lambda\pi}{2}-\pi\widetilde{T}\sqrt{1-\xi^2}\left(\frac{2\widetilde{t}}{\widetilde{T}}+1\right)\right]+\mathrm{sen}\left(\frac{\lambda\pi\widetilde{t}}{\widetilde{T}}\right)}{\frac{\sqrt{1-\xi^2}}{2\pi\widetilde{T}}\left(\lambda^2\pi^2-4\lambda\pi^2\widetilde{T}\sqrt{1-\xi^2}+\frac{4\pi^2\widetilde{T}^2}{\widetilde{H}(\widetilde{n})}\right)}\end{aligned} \tag{33}$$

$$\begin{aligned}\widetilde{Z}_{r,j}(\widetilde{n},\widetilde{t}) = {} & \frac{\left(\lambda\pi-2\pi\widetilde{T}\sqrt{1-\xi^2}\right)}{\exp\left[\pi\widetilde{T}\left(\frac{2\widetilde{t}}{\widetilde{T}}+1\right)(i\widetilde{n}+\xi)\right]}\frac{\exp\left[-2\pi\widetilde{T}(i\widetilde{n}+\xi)\right]\cos\left[\frac{\lambda\pi}{2}-\pi\widetilde{T}\sqrt{1-\xi^2}\left(\frac{2\widetilde{t}}{\widetilde{T}}+1\right)\right]-\cos\left[\frac{\lambda\pi}{2}+\pi\widetilde{T}\sqrt{1-\xi^2}\left(\frac{2\widetilde{t}}{\widetilde{T}}-1\right)\right]}{\frac{\sqrt{1-\xi^2}}{2\pi\widetilde{T}}\left(\lambda^2\pi^2-4\lambda\pi^2\widetilde{T}\sqrt{1-\xi^2}+\frac{4\pi^2\widetilde{T}^2}{\widetilde{H}(\widetilde{n})}\right)} \\ & + \frac{2\pi\widetilde{T}(i\widetilde{n}+\xi)}{\exp\left[\pi\widetilde{T}\left(\frac{2\widetilde{t}}{\widetilde{T}}+1\right)(i\widetilde{n}+\xi)\right]}\frac{\exp\left[-2\pi\widetilde{T}(i\widetilde{n}+\xi)\right]\mathrm{sen}\left[\frac{\lambda\pi}{2}-\pi\widetilde{T}\sqrt{1-\xi^2}\left(\frac{2\widetilde{t}}{\widetilde{T}}+1\right)\right]+\mathrm{sen}\left[\frac{\lambda\pi}{2}+\pi\widetilde{T}\sqrt{1-\xi^2}\left(\frac{2\widetilde{t}}{\widetilde{T}}-1\right)\right]}{\frac{\sqrt{1-\xi^2}}{2\pi\widetilde{T}}\left(\lambda^2\pi^2-4\lambda\pi^2\widetilde{T}\sqrt{1-\xi^2}+\frac{4\pi^2\widetilde{T}^2}{\widetilde{H}(\widetilde{n})}\right)}\end{aligned} \tag{34}$$

with δ_{2j} the Kronecker's delta and $\lambda = 2(j-2)$. Note that if $\gamma^* = 1$ $c_j = 0$ $\forall j$ leading to:

$$\widetilde{Z}(\widetilde{n},\widetilde{t}) = \widetilde{H}(\widetilde{n}) \tag{35}$$

References

Abd-Elaal, E.-S., Mills, J.E., Ma, X., 2013. An analytical model for simulating steady state flows of downburst. J. Wind Eng. Ind. Aerod. 115, 53–64.

Chay, M.T., Albermani, F., Wilson, R., 2006. Numerical and analytical simulation of downburst wind loads. Eng. Struct. 28, 240–254.

Davenport, A.G., 1967. Gust loading factors. J. Struct. Div. 93, 11–34.

Davenport, A.G., 1964. Note on the distribution of the largest value of a random function with application to gust loading. Proc. Inst. Civ. Eng. 28, 187–196. https://doi.org/10.1680/iicep.1964.10112.

Holmes, J.D., Oliver, S.E., 2000. An empirical model of a downburst. Eng. Struct. 22, 1167–1172. https://doi.org/10.1016/S0141-0296(99)00058-9.

Kwon, D.K., Kareem, A., 2019. Towards codification of thunderstorm/downburst using gust front factor: model-based and data-driven perspectives. Eng. Struct. 199, 109608.

Kwon, D.K., Kareem, A., 2013. Generalized gust-front factor: a computational framework for wind load effects. Eng. Struct. 48, 635–644.

Kwon, D.K., Kareem, A., 2009. Gust-Front factor: a new framework for wind load effects on structures. J. Struct. Eng. 135, 717–732.

Le, T.-H., Caracoglia, L., 2017. Computer-based model for the transient dynamics of a tall building during digitally simulated Andrews AFB thunderstorm. Comput. Struct. 193, 44–72.

Michaelov, G., Lutes, L.D., Sarkani, S., 2001. Extreme value of response to nonstationary excitation. J. Eng. Mech. 127, 352–363.

Ponte, J., Riera, J.D., 2010. Simulation of extreme wind series caused by thunderstorms in temperate latitudes. Struct. Saf. 32, 231–237.

Romanic, D., Nicolini, E., Hangan, H., Burlando, M., Solari, G., 2020. A novel approach to scaling experimentally produced downburst-like impinging jet outflows. J. Wind Eng. Ind. Aerod. 196, 104025 https://doi.org/10.1016/j.jweia.2019.104025.

Roncallo, L., Solari, G., 2020. An evolutionary power spectral density model of thunderstorm outflows consistent with real-scale time-history records. J. Wind Eng. Ind. Aerod. 203.

Roncallo, L., Solari, G., Muscolino, G., Tubino, F., 2022. Maximum dynamic response of linear elastic SDOF systems based on an evolutionary spectral model for thunderstorm outflows. J. Wind Eng. Ind. Aerod. 224, 104978 https://doi.org/10.1016/j.jweia.2022.104978.

Solari, G., 2016. Thunderstorm response spectrum technique: theory and applications. Eng. Struct. 108, 28–46.

Solari, G., 1993. Gust buffeting .2. Dynamic alongwind response. J. Struct. Eng. 119, 383–398.

Solari, G., 1983. Alongwind response estimation: closed form solution. J. Struct. Div. 108, 225–244.

Solari, G., Burlando, M., De Gaetano, P., Repetto, M.P., 2015a. Characteristics of thunderstorms relevant to the wind loading of structures. Wind Struct. An Int. J. 20, 763–791.

Solari, G., De Gaetano, P., Repetto, M.P., 2015b. Thunderstorm response spectrum: fundamentals and case study. J. Wind Eng. Ind. Aerod. 143, 62–77.

Solari, G., De Gaetano, P., Repetto, M.P., 2015c. Thunderstorm response spectrum: fundamentals and case study. J. Wind Eng. Ind. Aerod. 143, 62–77. https://doi.org/10.1016/j.jweia.2015.04.009.
Solari, G., Piccardo, G., 2001. Probabilistic 3-D turbulence modeling for gust buffeting of structures. Probabilist. Eng. Mech. 16, 73–86.
Solari, G., Repetto, M.P., Burlando, M., De Gaetano, P., Pizzo, M., Tizzi, M., Parodi, M., 2012. The wind forecast for safety management of port areas. J. Wind Eng. Ind. Aerod. 104–106, 266–277.
Zhang, S., Solari, G., De Gaetano, P., Burlando, M., Repetto, M.P., 2018. A refined analysis of thunderstorm outflow characteristics relevant to the wind loading of structures. Probabilist. Eng. Mech.
Zhou, Y., Kareem, A., 2001. Gust loading factor: new model. J. Struct. Eng. New York, N. Y. 127, 168–175. https://doi.org/10.1061/(ASCE)0733-9445(2001)127:2(168).